Lab on a Chip

PAPER

View Article Online
View Journal

Increasing hybridization rate and sensitivity of DNA microarrays using isotachophoresis†

Cite this: DOI: 10.1039/c4lc00374h

Crystal M. Han,[a] Evaldas Katilius[b] and Juan G. Santiago*[a]

We present an on-chip electrokinetic method to increase the reaction kinetics and sensitivity of DNA microarray hybridization. We use isotachophoresis (ITP) to preconcentrate target molecules in solution and transport them over the immobilized probe sites of a microarray, greatly increasing the binding reaction rate. We show theoretically and experimentally that ITP-enhanced microarrays can be hybridized much faster and with higher sensitivity than conventional methods. We demonstrate our assay using a microfluidic system consisting of a PDMS microchannel superstructure bonded onto a glass slide on which 60 spots of 20–27 nt ssDNA oligonucleotide probes are immobilized. Our 30 min assay results in an 8.2 fold higher signal than the conventional overnight hybridization at 100 fM target concentration. We show rapid and quantitative detection over 4 orders of magnitude dynamic range of target concentration with no increase in the nonspecific signal. Our technique can be further multiplexed for higher density microarrays and extended for other reactions of target-surface immobilized ligands.

Received 26th March 2014,
Accepted 20th May 2014

DOI: 10.1039/c4lc00374h

www.rsc.org/loc

1. Introduction

The DNA microarray is now a mature technology that enables investigation of several millions of probe sequences in parallel.[1] Its high-throughput capability and sensitivity have been leveraged in a wide range of applications including gene expression analysis,[2–4] diagnosis of diseases,[5–7] single nucleotide polymorphisms (SNPs),[8,9] and aptamer-based analysis of protein biomarkers.[10,11] DNA arrays use hybridization between targets suspended in a bulk sample solution and probes immobilized on a solid substrate. Despite its proven success, application of DNA arrays to rapid screening of samples remains a challenge.[12] In conventional microarray assays, the hybridization step alone typically requires overnight (15–24 h) incubation to yield a measurable signal from a wide range of target concentrations.[13,14] This constraint has impeded the application of microarrays to point-of-care applications where short sample-to-answer turnaround time is desirable. Reduction in hybridization time is also favorable because extended incubation times are associated with solution-dependent cleavage of the linkage chemistry between the probe and the solid support, negatively affecting the reproducibility and sensitivity.[15]

There are two main challenges in speeding up hybridization processes: overcoming the slow diffusion-limited target transport and the slow reaction rates associated with low target concentrations.[16] The vast majority of work toward speeding up DNA array hybridization has involved addressing the first of these limitations with active pumping and/or mixing of liquid solution containing the target molecules.[17] Successful microarray hybridization speed-up has been demonstrated using a wide variety of approaches. These include syringe pump-driven mixing,[18] microfluidic integrated peristaltic pump mixing,[19] mixing using 7 mm scale magnetic stirring bars,[20] pumping and mixing discrete sample plugs through serpentine microchannels,[21] acoustic microstreaming,[22] pumping with displacement micropumps,[23] centrifugal liquid pumping,[24–26] pneumatically driven mixing,[27,28] and electrokinetic sample dispensing and washing.[29]

The aforementioned methods of active pumping and vigorous mixing can increase the hybridization rate as they prevent hybridization from being diffusion limited by driving the fresh sample at its original concentration toward ligands on the surface. However, these approaches do not address the challenge of slow 2nd order reactions whose reaction rate is dictated by the kinetic parameters and trace concentration of targets. Kinetically limited reactions between suspended DNA and surface-bound cDNA can take hours to reach equilibrium due to the inherent dynamics of bulk-to-surface reactions (even assuming the perfect mixing).[30,31] Kinetically limited hybridization is therefore not addressed by pumping or mixing but rather by preconcentration of target species or methods of increasing kinetic parameters themselves (*e.g.*, by varying temperature). An example of preconcentration-driven microarray enhancement is the work of Edman *et al.*,[32] who reported a 30-fold increased hybridization rate by electrophoretically

[a] *Department of Mechanical Engineering, Stanford University, CA 94305, USA*
[b] *SomaLogic Inc., CO 80301, USA. E-mail: juan.santiago@stanford.edu*

† Electronic supplementary information (ESI) available. See DOI: 10.1039/c4lc00374h

accumulating DNA species at the capture probes immobilized on the surface of positively biased microelectrodes. This method received much attention for a brief time but has been largely abandoned by the field. We hypothesize that this abandonment is due to its strict requirement of microfabrication and the strong sensitivity of hybridization reactions to the effects of electrochemical reactions (which can damage DNA, dramatically change local pH, and/or generate bubbles).

Here we present a novel technique to accelerate and control microarray hybridization using isotachophoresis (ITP) focusing of targets. We use ITP to focus and transport target molecules over an array of probe sites in relatively simple microfluidic devices. ITP strongly increases the local target concentration and simultaneously enhances the local mixing through secondary flows and non-axial electric field components near the ITP focus zone.[33] ITP is an electrophoretic focusing technique, where target analyte ions are focused selectively between leading and trailing electrolyte ions of the two buffers. Relevant to the current work, ITP has been used to enhance the speed and sensitivity of 2nd order hybridization between suspended species. For example, Persat and Santiago[34] and Bercovici *et al.*[35,36] used ITP to enhance homogeneous DNA hybridization between a molecular beacon probe and its complementary target species demonstrating as much as 14 000 fold acceleration. Bahga *et al.*[37] showed detection of two target species sharing a common portion in their sequences by integrating ITP-enhanced hybridization with capillary zone electrophoresis. ITP has been also used to enhance the surface hybridization reaction between a suspended target and an immobilized probe. Garcia-Schwarz and Santiago[38,39] used ITP to speed up reactions between a single ssDNA species in solution and its complimentary capture probe immobilized into a polyacrylamide gel. In work published during the preparation of this manuscript, Karsenty *et al.*[40] showed an ITP aided reaction between a single target DNA and a single complementary cDNA immobilized on the surface of paramagnetic beads. Recently, Shkolnikov and Santiago[41] developed a spatiotemporal model for ITP-aided capture of analytes on a porous semi-infinite column, presented experimental validation of the model, and demonstrated ITP-aided sequence specific purification of a single DNA target from 10 000× abundant fish sperm DNA in a porous polymer monolith. However, we know of no studies toward integration of ITP with DNA arrays. Further, we also know of no studies combining ITP-enhanced reactions and multiplexed detection with more than two probe sequences.

In the current paper, we significantly extend the ITP-accelerated reactions to multiplexed detection of 20 target sequences using 60 spots of surface-immobilized probes (3 replicates for each target). We leverage high accumulation power of ITP to achieve both rapid and sensitive microarray hybridization. We present a simple analytical model for ITP hybridization, which predicts an order of 1000 fold speed up per column of spots and an approximately 10 fold increase in sensitivity compared to the kinetically limited reaction with no preconcentration. Our system consists of a single layer PDMS superstructure bonded to a glass slide containing a standard microarray with 60 probe spots exposed to the liquid within the PDMS channel. Our technique enables quantitative detection of 26 nt single-stranded DNA (ssDNA) over a dynamic range of 4 orders of magnitude. We experimentally demonstrate 30 min assay time with an 8.2 fold increase in sensitivity compared to conventional overnight microarray hybridization at 100 fM target concentration.

2. Overview of ITP-enhanced DNA array hybridization

Fig. 1a presents the schematics of our ITP-enhanced microarray hybridization assay performed in three steps: initial focusing, a diffusive homogenization step, and hybridization and transport. In the focusing step, we apply a relatively high electric field to rapidly extract DNA targets from the input reservoir and accumulate them at the moving ITP interface. The number of molecules accumulated in this step is determined by the volume of the focusing channel and buffer composition.[42,43] During this stage, a high electric field can cause some amount of Joule heating and electrokinetic flow instabilities[44] which result in non-uniform distribution of targets along the spanwise width of the channel (vertical direction in the figure). To correct this, the ITP zone is positioned within a narrow constriction in the channel wherein we deactivated the electric field for about 2 min. This process redistributes the sample *via* molecular diffusion. We then reapply a relatively low electric field, which avoids further

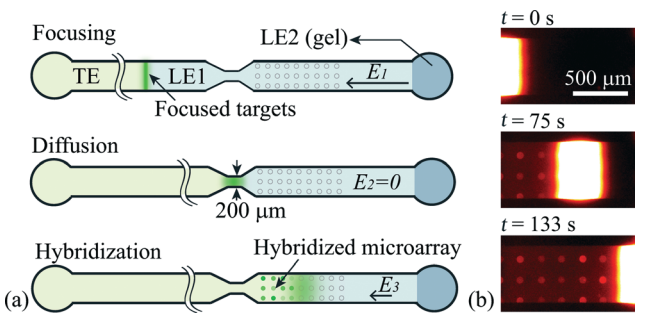

Fig. 1 Schematic and demonstration of ITP hybridization assay. (a) Illustration of the three step protocol of ITP hybridization: focusing, diffusion, and hybridization. Target ssDNA electromigrates and accumulates at the interface of TE and LE under a high electric field during the focusing step. When the ITP zone reaches the constriction of the channel, electric current is turned off, and diffusion redistributes target DNA for 2 min. In the subsequent hybridization step, a lower electric field is applied to avoid further instability, and the focused targets sweep over the immobilized probes. (b) Experimental demonstration of ITP microarray hybridization with fluorescence images taken three times. The ITP-focused Cy3 labeled ssDNA targets migrated on the surface immobilized complementary probes. After the ITP zone swept by, we observed that the specific fluorescence signal increases at the probe sites. The initial concentration of targets in this visualization was 100 pM. Note that these images are taken during the hybridization step of our method depicted in (a).

instabilities and migrates the focused targets at constant velocity over the microarray. See the ESI† for a visualization of ITP zones before and after the constriction shown in Fig. 1a. Microarray spots located immediately downstream of the constriction are exposed to highly focused target DNA for a finite, local residence time of the moving ITP zone (typically on the order of 50–250 s depending on the applied electric field). The hybridization reaction is greatly accelerated at the probe sites within the ITP zone, and the progression of the ITP zone downstream subsequently acts as an electrokinetic "wash" where unbound targets are removed from the probe spots and collected at the migrating ITP zone. After the sequence of events depicted in Fig. 1a, the channel containing the array is washed with wash buffers and dried in air prior to scanning on the microarray scanner.

3. Theory

We here present an analytical framework, which we used to compare ITP-enhanced surface hybridization with conventional hybridization. Our analysis also serves to guide the design and optimization of ITP hybridization experiments. In all cases, we model the surface binding reaction as a second order reaction with reaction off- and on-rate constants, k_{off} and k_{on}, respectively, and dissociation constant $K = k_{off}/k_{on}$. The reaction between an immobilized probe (P) and a suspended target (T) forming a hybrid species (H) can be expressed as follows:[45]

$$\text{(i) } \mathrm{P} + \mathrm{T} \underset{k_{off}}{\overset{k_{on}}{\rightleftharpoons}} \mathrm{H} \quad \text{(ii) } \frac{d\tilde{C}_H}{dt} = k_{on} C_T \left(\tilde{C}_{H0} - \tilde{C}_H\right) - k_{off} \tilde{C}_H \qquad (1)$$

where $\tilde{C}_H$ and $\tilde{C}_{H0}$ denote molar surface concentration of hybrid pairs and of free binding sites at $t = 0$ in units of mol m^{-2}, respectively. C_T is the volumetric target concentration at the immediate vicinity of the immobilized probes with units of mol m^{-3}. The value of C_T is determined by convection–diffusion processes in the bulk liquid.

We here develop an approximate relation to characterize these reactions in the limit of perfect mixing where hybridization is entirely limited by reaction kinetics. In this regime, target concentration remains unchanged from the initial concentration, C_{T0}, everywhere above the immobilized probes at all times. Therefore, substituting C_{T0} for C_T in eqn (1-ii) yields the solution for the fraction of surface probes hybridized expressed as:

$$h_{kin} = \frac{C_0^*}{C_0^* + 1}\left(1 - \exp\left(-\left(C_0^* + 1\right) k_{off} t\right)\right) \qquad (2)$$

where $C_0^* = C_{T0}/K$ and h_{kin} denotes the fraction of the hybridized immobilized probe defined as $\tilde{C}_H/\tilde{C}_{H0}$. This is a well-established analytical solution for kinetically limited hybridization reactions applicable to well-mixed cases.[46–48] From eqn (2), the fraction of hybridized probes at the equilibrium, h_{eq}, can be easily derived by setting $t \to \infty$:

$$h_{eq} = \frac{C_0^*}{C_0^* + 1} \qquad (3)$$

The above relation shows that the fraction of the hybridized probe at equilibrium is directly proportional to the initial target concentration for cases of $C_0^* \ll 1$, which is the desired design criterion for quantitative microarray analyses. Further, the initial target concentration limits the theoretical maximum signal of the assay. This limitation has prompted the use of long incubation times, in efforts to approach thermodynamic equilibrium and maximize sensitivity.[49,50] We note that eqn (3) is also applicable to the equilibrium state of diffusion-limited reactions under the assumption that spots consume negligible amounts of the target from the solution through binding reactions.[51]

We model ITP hybridization assay as a kinetically limited reaction at an elevated, characteristic target concentration associated with the ITP preconcentration. Increased concentration both improves the rate of capture and increases the maximum signal attainable from a given target concentration. ITP is also known to cause secondary flows[33] and these help avoid diffusion-limited regimes. We assume that ITP-enhanced surface hybridization is kinetically limited because the typical ITP hybridization time scale (residence time of ITP zone) is smaller than the time scale of depletion zone formation, which indicates the onset of the diffusion limitation. We verified the validity of this assumption using typical parameter values for our system and extrapolating from Pappaert and Desmet's[51] nondimensional analysis on heterogeneous DNA hybridization. We summarize the values of the typical parameters for our system in Table 1, and with these we calculate the five dimensionless numbers, identified in Pappaert and Desmet's work,[51] and summarize these in Table 2. *Da* is the Damkohler number defined as the ratio of the reaction rate to the diffusive mass transfer rate. C_0^* denotes the ratio of the maximum forward to backward reaction rate. α is the ratio of the spot radius to the fluid layer height, and C_0' is the ratio of the number of targets in solution above the spot to the number of binding sites in the spot at $t = 0$. Lastly, τ is a dimensionless reaction time for ITP hybridization.

Table 1 Typical parameter values for our ITP hybridization in SI units

Parameter	Name	Value
D_{mol}	Molecular diffusion coefficient for target lengths 20–27 nt	9.2×10^{-10} m^2 s^{-1} (ref. 52 and 53)
k_{on}	Kinetic on-rate constant	76 m^3 (mol s)$^{-1}$
k_{off}	Kinetic off-rate constant	4.4×10^{-5} s^{-1}
K	Dissociation constant	5.7×10^{-7} mol m^{-3}
a	Array spot radius	3.0×10^{-5} m
d	Channel height	4.0×10^{-5} m
$\tilde{C}_{H0}$	Molar surface concentration of immobilized probes	2×10^{-9} mol m^{-2}
C_{T0}	Reservoir concentration of target	10^{-9} mol m^{-3}
t_{ITP}	ITP hybridization time	235 s
p	ITP fold preconcentration level	549

Table 2 Estimates of nondimensional parameters as defined by the analysis of Pappaert and Desmet[51] and evaluated using the values given in Table 1

Nondimensional parameter	Estimation
$Da = \frac{k_{on}\tilde{C}_{H0}d}{D_{mol}}$	0.07
$C_0^* = \frac{C_{T0}^* k_{on}}{k_{off}}$	0.0017
$\alpha = \frac{a}{d}$	0.75
$C_0' = \frac{C_{T0}d}{\tilde{C}_{H0}}$	2×10^{-5}
$\tau = k_{off}(1 + pC_0^*)t_{ITP}$	0.01

Pappaert and Desmet[51] plot the fraction of hybridized probes *versus* dimensionless time for their numerical solution of the microarray surface reaction problem for values of C_0' ranging from 10^{-5} to 10^{-1}. The transition from the reaction-limited phase to the diffusion-limited phase can be found as the time when the numerical solution deviates from the kinetically limited analytical solution. Based on their solution for $C_0' = 1 \times 10^{-5}$, we estimate that the dimensionless transition time is 0.01 for ITP hybridization associated with $C_0' = 2 \times 10^{-5}$. Other nondimensional parameters used in their solution were $C_0^* = 10^{-3}$, $\alpha = 5$, and $Da = 1$. In comparison, our α is 7 fold lower and Da is 14 fold lower, while C_0^* is approximately the same. The same paper by Pappaert and Desmet[51] also showed that the transition time from kinetic- to diffusion-limited regime is increased for lower Da and α. The latter suggests that the dimensionless transition time associated with our parameters may be longer than 0.01, implying that the reaction stays longer in the kinetically limited regime. Thus we conclude that the dimensionless ITP reaction time, 0.01, is smaller than the transition time to the diffusion limited phase, hence ITP hybridization is kinetically limited.

As a simple approximation, we model the concentration profile of ITP focused targets as a top-hat pulse with a characteristic target concentration value of pC_{T0} and a characteristic ITP zone width of δ_{ITP}, traveling at a known, constant velocity of V_{ITP}. Here p denotes the fold preconcentration level of the target species in the ITP zone compared to the reservoir concentration. Using this simple model of an ITP zone, we estimate the duration during which an immobilized probe is exposed to the high concentration target as the form $t_{ITP} = \delta_{ITP}/V_{ITP}$. That is, we model that ITP hybridization is performed at a concentration of pC_{T0} for a short, finite ITP reaction time of t_{ITP}, during which the reaction is yet kinetically limited. We derive an approximate analytical model for ITP hybridization by simply substituting pC_{T0} for C_{T0} and t_{ITP} for t in eqn (2) to obtain

$$h_{ITP} = \frac{pC_0^*}{pC_0^* + 1}\left(1 - \exp\left(-\left(pC_0^* + 1\right)k_{off}t_{ITP}\right)\right), \quad (4)$$

where h_{ITP} denotes the fraction of surface probes hybridized after the ITP zone passes. This simple model gives insight into ITP-aided hybridization dynamics and will serve as a comparison case for the well-mixed surface hybridization with no preconcentration. We will use these analytical models to characterize ITP enhanced hybridization in comparison to kinetically limited hybridization. A similar analysis on the ITP hybridization was provided recently by Karsenty *et al.*[40]

4. Materials and methods

4.1. Buffers, reagents and DNA sequences

We used twenty synthetic target–probe molecule pairs composed of perfectly complementary DNA and cDNA. We provide sequences of target and probe DNA oligonucleotides in the ESI.† We arbitrarily named target–probe pairs as numbers from 1 to 20. The target sequences were synthesized with a Cy3 dye at the 5′ terminus. Capture probes were synthesized with the amine group on a C6 linker at the 5′ end with an additional hexa-ethylene glycol linker (HEG) that separates amine group from the DNA sequence. Targets and the respective partner probes had the same length ranging from 20 to 27 nt. Additionally, we purchased and used as corner markers synthetic DNA with the amino modifier C6 at the 5′ terminus and Cy3 at the 3′ terminus. All oligonucleotides were purchased from Integrated DNA Technologies (IDT, Coralville, IA), and 100 μM of their stock solutions were stored at −20 °C.

For ITP hybridization, the aqueous LE buffer inside the channel, LE1, contained 250 mM HCl, 500 mM Tris, 5 mM $MgCl_2$, 0.1% w/w 1 MDa poly(vinylpyrrolidone) (PVP), 10% formamide, and 0.01% w/w Tween20. We chose the concentration of HCl and Tris as a good compromise between strong ITP focusing and Joule heating. The gel-phase LE buffer in the LE reservoir, LE2, was composed of 250 mM HCl, 500 mM Tris, and 25% w/v Pluronic F-127. At 25% concentration of Pluronic F-127, the solution is in liquid form below +4 °C but quickly changes to the solid-phase as it is transferred to the reservoir and exposed at room temperature.[54] We used this thermal gelation property to prevent pressure driven flow in the channel during ITP.[43,55] The aqueous TE buffer contained 25 mM HEPES, 50 mM Bis–tris, 1% PVP, and varying concentrations of a mixture of ssDNA targets. The loading volume of the TE buffer in the reservoir was 20 μl. Thus we used 2 attomoles of each sequence for the hybridization of 100 fM target concentration. For conventional hybridization, target DNA was mixed with the LE1 buffer to final concentrations ranging from 100 fM to 10 nM. We used a total of 21.6 μl of the LE1 buffer for each experiment, and we estimate that the channel contained only 1.6 μl. So, for example, 2 attomoles and 0.16 attomoles of each target sequence were used, respectively, in the reservoirs and in the channel for the 100 fM target concentration experiments.

HCl, HEPES, Tris, Bis–tris, $MgCl_2$, Pluronic F-127, and Tween20 were purchased from Sigma-Aldrich (St. Louis, MO). PVP was obtained from Polysciences, Inc. (Warrington, PA). Formamide was purchased from Invitrogen (Grand Island, NY).

All solutions were prepared with UltraPure DNase free distilled water (GIBCO Invitrogen, Carlsbad, CA).

4.2. Microarray

The microarrays were custom designed and manufactured by Applied Microarrays, Inc. (AMI, Tempe, AZ) using proprietary non-contact piezoelectric spotting equipment. Glass slides with epoxysaline coating (Schott Nexterion Slide E, Elmsford, NY) were used as the substrates for immobilization. Each slide had 6 identical microarrays; each array consists of 8 repeated spots for 20 probe sequences (a total of 160 spots). The spot diameter was 60 μm, and the center-to-center distance between spots was 150 μm. The corner marker DNA was immobilized to indicate the location and the direction of the microarrays. The detailed array geometry is described in the ESI.† Since we purchased blocked arrays, we performed no further blocking before hybridization. Once opened from their packaging, we stored the unused microarrays in a vacuum chamber (Bel-Art Scienceware, Wayne, NJ).

4.3. Fabrication of the microfluidic device

We designed a single layer polydimethylsiloxane (PDMS) microfluidic superstructure. When bonded to the microarray glass substrate, this structure created a simple channel over the array consisting of an inlet and an outlet reservoir. This simple structure was used to extract target DNA from the inlet, focus it, and perform rapid ITP hybridization. We used the identical PDMS and glass substrate system to perform conventional hybridization without ITP or mixing. The fluidic microchannel was 80 mm long and had a uniform depth of 40 μm. The channel had a 500 μm width, except for a smooth, 200 μm wide constriction fabricated into the region just upstream of the probe sites. Optimized, low-dispersion turns (not shown in Fig. 1) were also used to minimize dispersion of the sample at turns.[55,56]

We used a SU-8 master mold fabricated by the Stanford Microfluidics Foundry (Stanford, CA) as a positive cast for the microfluidic superstructure. To optimize bonding, we experimented with several ratios of the precursor-to-curing agent (Sylgard 184, Dow Corning, Menlo Park, CA) and found that a ratio of 20 : 1 (w/w) formed a spontaneous seal between the PDMS slab and epoxysaline-coated glass slide with no plasma treatment. We degassed the reagents for 30 min, thoroughly mixed, poured into the mold, and cured at 65 °C for at least 6 h. We then peeled off the PDMS slab and punched holes to form inlet and outlet reservoirs. We manually aligned the PDMS superstructure and microarray slide based on the alignment markers on the PDMS and created a reversible contact bond between them. We observed no leakage of these bonds. The final microfluidic system contained 40–60 spots within the fluidic channel, depending on the alignment.

4.4. ITP hybridization and conventional hybridization

Immediately before each experiment, we primed a channel by flushing with 50% ethanol (Sigma-Aldrich, St. Louis, MO) for 5 min. This mitigated problems with air bubble formation during filling.[57] We dried the ethanol by flowing air with a vacuum line for 2 min before filling the channel with LE1. As depicted in Fig. 1a, ITP hybridization required three buffers: LE1, LE2, and TE. After filling the entire channel with LE1 buffer, we rinsed the two reservoirs using distilled water and emptied the reservoirs thoroughly with vacuum. We pipetted 20 μL of aqueous TE buffer and gel-phase LE buffer (LE2) into the input and output reservoirs, respectively. We then placed platinum wire electrodes into each reservoir. The LE2 buffer changed from the liquid to solid phase immediately after it was pipetted into the well from the ice bath, preventing unwanted pressure driven flow. We initiated ITP enhanced hybridization experiments by applying 1100 V to the LE well and grounding the TE well using a high voltage source meter (2410, Keithley Instruments, Cleveland, OH). We turned off the field as the ITP zone arrived at the constriction and waited for 2 min. Hybridization was then performed at room temperature by applying constant currents. For visualization experiments shown in Fig. 1b, we applied 4 μA while we applied 2 μA for all other experiments. Higher currents result in a shorter assay time but lower sensitivity (as residence time over each spot is decreased). For all quantitative experiments, we selected 2 μA as a good compromise between the duration and sensitivity of assay.

For conventional hybridization experiments, we primed a channel in the same way, filled it with the LE1 buffer containing target DNA, and then filled the two reservoirs with 10 μl of the same buffer. We taped a PCR sealer film (Microseal B Adhesive Sealer, MSB-1001, Bio-Rad) on top of the PDMS superstructure to prevent evaporation and wrapped the entire device with aluminum foil. The microfluidic system was then incubated at room temperature for 15 h.

After each ITP and conventional hybridization experiment, we emptied both reservoirs and filled the channel with 1× saline-sodium citrate (SSC, Invitrogen, Carlsbad, CA) for 1 min, then completely dried the channel by flowing air with a vacuum line for 2 min. We then peeled off the PDMS channel superstructure and carried out an additional two-step washing inside a 50 ml centrifuge tube. For the latter, the microarray slide was first immersed in a solution containing 0.1× SSC and 0.1% w/w TritonX (Sigma-Aldrich St. Louis, MO) for 1 min and then transferred to 0.1× SSC for an additional 1 min incubation. At the end of this series of washing, we dried the microarray slides completely by blowing air from a duster type compressed gas can.

4.5. Detection

For the on-chip visualization of microarray hybridization shown in Fig. 1b, we used an inverted epifluorescence microscope (Eclipse TE300, Nikon, Tokyo, Japan) equipped with a 10× objective (Plan, NA 0.45, Nikon, Tokyo, Japan). We used a mercury lamp and a filter cube (XF102-2, Omega Optical, Brattleboro, VT) for excitation of a Cy3 fluorophore. We recorded images with generation III, intensified CCD camera

(IPentaMAX; Roper Scientific, Trenton, NJ), controlled with Winview32 (Princeton Instruments, Trenton, NJ).

For all other results presented here, we scanned the microarray slides using a GenePix 4000B array scanner (Axon Instrument, CA) located in Stanford Functional Genomic Facilities (SFGF, Stanford, CA). We used hardware settings of 100% laser power, 5 μm resolution, and either 400 or 800 PMT gain. We used GenePix Pro 6.0 software (Axon Instrument, CA) to extract images and obtain quantitative estimates of the fluorescence intensity from each spot.

5. Results and discussion

5.1. Demonstration of microarray hybridization acceleration

We first performed on-chip visualization experiments of the ITP hybridization process using standard epifluorescence microscopy with CCD camera imaging. In Fig. 1b, we present images taken from a single ITP microarray hybridization experiment conducted three times at a fixed location. Here, we focused twenty Cy3 labeled ssDNA target sequences at 100 pM initial concentration and let the ITP zone sweep over the immobilized probe spots. Initially, the probes were in contact with the aqueous LE1 solution containing no target species, thus we observed no fluorescence signal. After the ITP zone passed over the reaction spots, we observed a fluorescence intensity increase, as expected. The background signal in these images is higher in the trailing zone of the ITP peak as the TE here contains target species. These images serve as a qualitative description of the assay.

5.2. Experimental conditions and parameters required for our model predictions

Our analytical model predicts that preconcentration with ITP can enhance hybridization in three ways: speeding up the reaction, improving sensitivity, and enabling quantitative detection. First, the speed-up in the rates of hybridization reaction by ITP preconcentration scales with p (*e.g.*, which can be seen by taking the derivative of eqn (4) with respect to t_{ITP}) compared to kinetically limited hybridization without preconcentration. As usual with reaction acceleration schemes for microarrays, we compare the time to obtain the same signal intensity from both methods. To this end, we calculate 99% characteristic time, *i.e.*, the time required to reach 99% of the equilibrium signal, h_{eq}, defined in eqn (3) for a given target concentration. In Fig. 2, dashed contour lines represent the ratio of kinetically limited hybridization time to ITP hybridization time. For a common range of p and C_0* values presented here, we see that an order of 1000-fold speedup is predicted.

Second, we predict an increase in sensitivity for ITP enhanced hybridization. In Fig. 2 solid contour lines represent the ratio of the fraction hybridized of hybridization with and without ITP *versus* the nondimensional time, $k_{off}t_{ITP}$, and the preconcentration level, p. A ratio higher than unity is achieved for the range of parameters highlighted by the gray area. For example, for a typical k_{off} value of order 10^{-4} s^{-1},

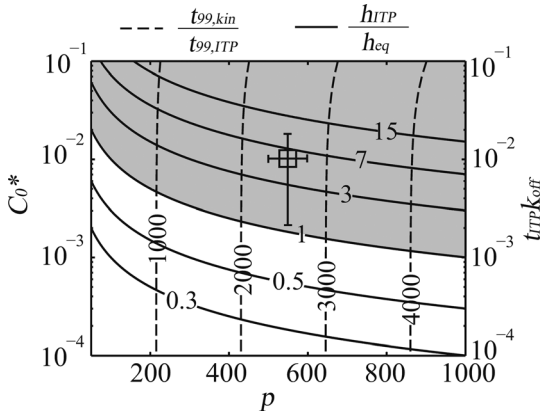

Fig. 2 Comparison of sensitivity and hybridization time between ITP and well-mixed (kinetically limited) surface hybridizations. Dashed contours represent the ratio of characteristic time to reach 99% of the equilibrium with kinetically limited reaction to that with ITP, $t_{99,kin}/t_{99,ITP}$, for a common range of C_0* and p. We defined C_0* as a dimensionless parameter, C_0/K. Solid contour lines represent the ratio of the fraction of hybridized probes of ITP hybridization to that from the well-mixed case at equilibrium, h_{ITP}/h_{eq}, and are plotted for relevant values of nondimensional time $t_{ITP}k_{off}$ and p. For the solid lines, we set C_0* at 10^{-4}, but we note that these contours have a negligible dependence on C_0* for C_0* $< 10^{-2}$. The gray area represents the range of parameters $t_{ITP}k_{off}$ and p which result in an ITP assay with higher sensitivity than the kinetically limited reaction. The square symbol represents the model prediction for the estimated experimental conditions used in Fig. 3 and 4 (p = 549, t_{ITP} = 235 s, and k_{off} = 4.4×10^{-5} s^{-1}), and h_{ITP}/h_{eq} is 5.6 under these conditions. The uncertainty bars on this point represents 95% confidence intervals based on a propagation of error analysis.

residence times of 50 s or greater result in h_{ITP}/h_{eq} values greater than unity for preconcentration factors of about 300 or greater. Such preconcentration values and residence times are easily achievable with ITP for a wide variety of targets and sample types.[43] We note that the abscissa and ordinate coordinates of Fig. 2 are not completely orthogonal since p and t_{ITP} are both functions of the electric field. We chose this representation because these dimensionless parameters facilitate comparison with experimental conditions. We refer the readers to the ESI† for an alternate contour plot showing explicitly the effect of the electric field on the ratio of the fraction hybridized of ITP and conventional hybridization.

Third, ITP hybridization enables quantitative detection for a wide dynamic range, fulfilling a primary criterion as an analytical technique. For conventional hybridization at equilibrium, the fraction of the hybridized probe is directly proportional to the initial target concentration, $h_{kin} \approx C_{T0}/K$ for conditions satisfying C_0* $\ll 1$. Similarly, in ITP hybridization, a Taylor series expansion for the limiting case of $(pC_0* + 1)k_{off}t_{ITP} \ll 1$ yields the linear proportionality of $h_{ITP} \approx pk_{on}t_{ITP}C_{T0}$. In both cases, the assays result in a linear relation between the initial target concentration and the fraction hybridized h. However for the conventional hybridization case, an absolute amount of the captured target depends on calibration for a sequence specific equilibrium constant K, whereas it depends on the product of $pk_{on}t_{ITP}$ for the ITP

case. The latter includes both a sequence-specific parameter k_{on} and an ITP condition parameter pt_{ITP}. This offers flexibility in assay design as we have found that ITP conditions can be easily controlled and very reproducible. In summary, conventional hybridization relies on achieving near-equilibrium using long incubation times (and appropriate mixing) for some initial target concentration. Its sensitivity and time are therefore typically limited by K and either a slow reaction rate or a slow diffusion time. In contrast, ITP strongly promotes the forward reaction by preconcentration (and mixing *via* secondary flow). Therefore despite the shorter reaction time, ITP's preconcentration can achieve a higher value of the hybridized molecule fraction, h. Our protocol then effectively "freezes" this higher value of h by drying out (with air) the reaction surface.

We next describe the experimental conditions and dimensional parameters we required to apply to our analytical model. We measured the ITP velocity, V_{ITP}, ITP interface width, δ_{ITP}, and preconcentration level, p, from independent ITP hybridization experiments (N = 5). For these calibration experiments, we obtained images of the migrating ITP zone containing twenty Cy3 labeled targets (each with 250 pM reservoir concentration) under a 2 μA constant current condition with an ICCD gain of 40, exposure time of 1 s, and 0.1 Hz frame rate. Note that here we used the same experimental conditions associated with Fig. 3 and 4 below. We first performed image analysis on the raw image (I) to subtract the background intensity (BG) and correct the non-uniform illumination by flat field image (FF) according to an equation of the form:

$$I_{corr} = \frac{I - BG}{(FF - BG)/\max(FF - BG)}, \quad (5)$$

where I_{corr} denotes the corrected intensity of the image. We experimentally observed that the ITP concentration profile was approximately Gaussian in shape. We fit the experimental data with Gaussian distribution of the form $Ae^{(x-\mu)^2/2\sigma^2}$, where A is the amplitude, μ is the mean, and σ is the standard deviation (*cf.* Fig. S4b for experiment *vs.* Gaussian fit *vs.* top hat approximation in the ESI†). Our titration experiments resulted in a calibration equation of the form $I_{corr} = 1.02 \times 10^{10} C_{T0} + 41$ (see the ESI†) to convert the corrected intensity of the ITP zone into concentration of targets. In our analytical model, we approximated the ITP concentration profile as a top-hat pulse with a characteristic ITP interface width, δ_{ITP}. To this end, we set δ_{ITP} to be the $\pm 2\sigma$ width of the Gaussian peak. We determined the magnitude of the top-hat pulse, pC_{T0}, such that the area under the pulse, $4\sigma pC_{T0}$, was equal to the area under the Gaussian peak, $\sqrt{2\pi}A\sigma$. This provided the estimate for the ITP zone width and preconcentration level; δ_{ITP} = 746 ± 32 μm and p = 549 ± 49. Further, the ITP velocity was measured by dividing the average displacement distance of the Gaussian fit obtained from thirty pairs of images taken with 10 s image-to-image delays. The estimated

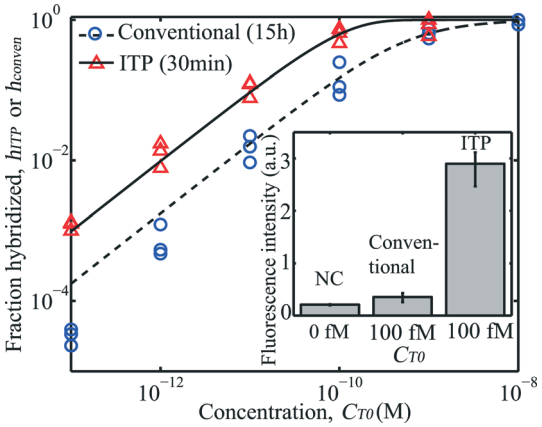

Fig. 3 Experimental data demonstrating quantitative and sensitive detection of a target sequence using ITP microarray hybridization and its comparison to conventional array hybridization. Titration curves shown here were obtained for 26 nt ssDNA (target 1) concentrations ranging from 100 fM to 10 nM. Along with experimental data (symbols), we show results of analytical models with a single fitting parameter for the conventional (dashed) hybridization and an additional fitting parameter for the ITP case (solid). The inset compares raw fluorescence intensity from C_{T0} = 100 fM hybridization data of both methods and the negative control with no target. The increase of fluorescence intensity over the negative control was 1.7 for conventional hybridization and 14 for ITP hybridization. ITP creates an 8.2 fold increase in sensitivity and a 30 fold decrease in assay time. The range bar in the inset is used to indicate maximum and minimum values of data points across repetitions (N = 3).

value of V_{ITP} at 2 μA was 3.2 ± 0.05 μm s^{-1}. Dividing the value of δ_{ITP} by V_{ITP}, we obtained the characteristic ITP reaction time as t_{ITP} = 235 ± 12 s. For all ITP parameters, we reported mean values from five experiments along with 95% confidence interval based on the Student's t-distribution.

Next, we used the measured ITP parameters and estimated kinetic parameters $K = 5.7 \times 10^{-10}$ M and $k_{off} = 4.4 \times 10^{-5}$ s^{-1} (see section 5.3) to obtain the model prediction of speed-up and sensitivity increase for our experiments. We show the predictions with a square symbol in Fig. 2. Our simple theory predicts increase in sensitivity of order 5.6 fold, while we experimentally observe an 8.2 fold increase in the signal (see section 5.3). As shown with the experiments, ITP's high accumulation power can easily achieve sensitivity improvement over hybridization methods without preconcentration. Further, we compare the assay time of hybridization with and without ITP preconcentration. The 99% characteristic time for well mixed and ITP hybridization are 28.7 h and 41 s, respectively, using C_0^* = 0.01, which implies 5.7 pM. This indicates that the speedup in ITP hybridization constitutes 2500 fold for each column of spots in the microchannel (along the spanwise direction). For multiple columns, the total ITP hybridization time is increased by the ratio of the total length of the array to the ITP zone width δ_{ITP}.

5.3. Rapid, quantitative and high-sensitivity detection

We demonstrate wide quantitative detection dynamic range, high sensitivity, and hybridization acceleration of our

technique by comparing titration curves for ITP and conventional hybridization with no mixing. In Fig. 3, we present experimental data of the fraction of hybridized probes against six concentrations for ITP (triangle) and conventional hybridization (circle) cases. The hybridization experiments were performed using a mixture of twenty target sequences with initial/reservoir concentrations varying from 100 fM to 10 nM. Here we show results from only target 1, but we include additional data analyses for other targets in the ESI.† There, we also provide a discussion on the limit of detection and experiment-to-experiment reproducibility of our method. The fraction of the hybridized probe was estimated from experiments by normalizing the background-subtracted fluorescence signal with the maximum value for the respective methods. In both cases, we observed that the fraction of the hybridized probe proportionally increased with increasing concentration over a dynamic range of 4 orders of magnitude. The fraction hybridized for ITP hybridization was higher than that of conventional hybridization for all concentrations, showing improved sensitivity by the preconcentration effect of ITP. For example at 100 fM, the average fraction hybridized for the ITP and conventional hybridizations were 1.2×10^{-3} and 3.2×10^{-5}, respectively. Multiplying the values with the probe surface density and spot dimension given in Table 1, we calculate that the ITP hybridization recovered 6.7×10^{-21} moles (4.0×10^{3} copies) and conventional hybridization recovered 1.8×10^{-22} moles (1.1×10^{2} copies). ITP has approximately 1 order of magnitude higher capture amount than conventional hybridization. In the inset, we compare the raw fluorescence intensities for ITP and conventional hybridization (here, without background subtraction) for the lowest concentration case (100 fM) and a negative control of no target in solution. The intensity increase relative to the negative control was 1.7 for conventional hybridization and 14 for ITP hybridization, which translates to an 8.2 fold increase in sensitivity for ITP hybridization. The ITP assay total duration (for all spots) was 30 min, compared to 15 h for the conventional hybridization; hence the increased sensitivity was accompanied by a 30-fold speed up for the process.

Shown together with the experimental data set are analytical models for the conventional and ITP hybridizations (dashed and solid lines). To obtain these theoretical curves, we first fit the conventional hybridization data with the equilibrium model of eqn (3) using K as a single, global fitting parameter. The fitting parameter was determined as $K = 5.7 \times 10^{-10}$ M using the 'nlinfit' nonlinear fitting function of Matlab. For the ITP model, we used the same value of K combined with independently measured estimate values of $p = 549$ and $t_{ITP} = 235$ s from section 5.2. A single additional fitting parameter for the ITP hybridization predictions was determined as $k_{on} = 7.6 \times 10^{4}$ M^{-1} s^{-1}. These hybridization parameter values are typical for heterogeneous hybridization.[31,58,59] For ITP, we observed a good qualitative agreement of predicted trends and our experimental data. For conventional hybridization, we observed a good qualitative agreement at higher concentrations but a slight discrepancy at concentrations below 1 pM. We hypothesize that the overprediction by the model of the fraction hybridized is due to the fact that the conventional hybridization did not reach equilibrium despite its 15 h incubation. We believe that hybridization is diffusion limited at these low target concentrations and thus requires longer time to reach equilibrium.[50,60]

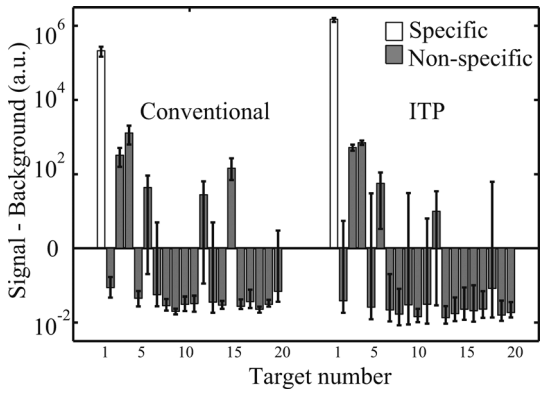

Fig. 4 Comparison of specific and nonspecific signals between conventional and ITP hybridizations. The background subtracted fluorescence signal for each target on a log scale is plotted. We here hybridized target 1 alone at 100 pM concentration and measured the fluorescence intensity from all of the 20 probe sequences across the 60 spots (3 spots per sequence). Data shown are the average intensities from three experiments with range bars representing the absolute range of measured values. A negative value of the background-subtracted intensity indicates that non-specific binding was not observed. The ratio of the specific signal to the highest nonspecific signal was 160 for conventional hybridization and 2130 for ITP hybridization.

5.4. Comparison of the non-specific signal for ITP and conventional hybridization

In Fig. 4, we present measurements of specific and non-specific signals obtained with conventional and ITP hybridizations. For this demonstration, we included only one target (target 1) at an initial concentration of 100 pM and performed conventional and ITP-aided hybridizations. After hybridization, we recorded the raw fluorescence intensity from all 20 probe sequences. The bar plots represent the background-subtracted fluorescence intensity resulting from specific (for target 1, white) and nonspecific (for target numbers 2–20, gray) hybridizations. For most of the sequences, the non-specific signal was lower than the local background signal, indicating negligible non-specific binding of DNA or dye to the array surface. To obtain a quantitative measure for specificity, we calculated a specificity index defined as the ratio of the specific signal to the highest nonspecific signal (target 4). The specificity index was 160 for conventional hybridization and 2130 for ITP hybridization. The more than 10 fold increase in the specificity index was achieved mainly by the increased specific signal of ITP hybridization. Importantly, the nonspecific signals for both conventional and ITP hybridizations were of the same order of magnitude. This confirms that ITP hybridization enables

sensitivity increase with no negative effects on the specificity of the assay.

6. Conclusions

We demonstrated the acceleration and sensitivity improvement of DNA microarray hybridization using ITP. Our method leverages high preconcentration power of ITP to overcome the slow reaction kinetics of surface hybridization. We focus target molecules into a narrow (order 100 μm) ITP zone, transport them over immobilized probes, and speed-up the surface binding reaction. Our approach enabled 30 fold shorter hybridization assay time compared to the overnight conventional hybridization and at the same time improved the sensitivity by nearly 1 order of magnitude without increasing the nonspecific signal. The current paper is also the first ITP-based hybridization work demonstrating the quantitative analysis for significant multiplexing (here 20 sequences across a total of 60 spots). We believe that our technique can be easily adapted for a high density DNA array by upscaling the dimensions of the device. Furthermore, the current study can be merged with ITP's nucleic acid extraction functionality to create an integrated on-chip nucleic acid analysis system that inputs complex sample and outputs multiplexed quantitation of sequences (*e.g.*, without amplification). We hypothesize that the method presented here is generally applicable to accelerate other target–receptor binding processes such as antigen–antibody, protein–aptamer, and aptamer–cDNA. Rapid and sensitive ITP microarray hybridization shows the potential to speed-up traditionally long processes of biomarker discovery, clinical diagnosis, and SNP analyses.

Acknowledgements

We gratefully acknowledge support from Defense Advanced Research Projects Agency (DARPA) under contract number HR0011-12-C-0080. C.M.H. gratefully acknowledges the Robert and Katherine Eustis Stanford Graduate Fellowship for support.

References

1 D. Okou, K. Steinberg and C. Middle, *Nat. Methods*, 2007, **4**, 1109–1111.
2 D. T. Ross, U. Scherf, M. B. Eisen, C. M. Perou, C. Rees, P. Spellman, V. Iyer, S. S. Jeffrey, M. Van de Rijn, M. Waltham, A. Pergamenschikov, J. C. Lee, D. Lashkari, D. Shalon, T. G. Myers, J. N. Weinstein, D. Botstein and P. O. Brown, *Nat. Genet.*, 2000, **24**, 227–235.
3 A. Adomas, G. Heller, A. Olson, J. Osborne, M. Karlsson, J. Nahalkova, L. Van Zyl, R. Sederoff, J. Stenlid, R. Finlay and F. O. Asiegbu, *Tree Physiol.*, 2008, **28**, 885–897.
4 M. Schena, D. Shalon, R. W. Davis and P. O. Brown, *Science*, 1995, **270**, 467–470.
5 J. Marx, *Science*, 2000, **289**, 1670–1672.
6 R. W. Wallace, *Mol. Med. Today*, 1997, **3**, 384–389.
7 Y. Shen and B.-L. Wu, *Clin. Chem.*, 2009, **55**, 659–669.
8 J. G. Hacia, J. B. Fan, O. Ryder, L. Jin, K. Edgemon, G. Ghandour, R. A. Mayer, B. Sun, L. Hsie, C. M. Robbins, L. C. Brody, D. Wang, E. S. Lander, R. Lipshutz, S. P. Fodor and F. S. Collins, *Nat. Genet.*, 1999, **22**, 164–167.
9 X. Chen and P. F. Sullivan, *Pharmacogenomics J.*, 2003, **3**, 77–96.
10 L. Gold, D. Ayers, J. Bertino, C. Bock, A. Bock, E. N. Brody, J. Carter, A. B. Dalby, B. E. Eaton, T. Fitzwater, D. Flather, A. Forbes, T. Foreman, C. Fowler, B. Gawande, M. Goss, M. Gunn, S. Gupta, D. Halladay, J. Heil, J. Heilig, B. Hicke, G. Husar, N. Janjic, T. Jarvis, S. Jennings, E. Katilius, T. R. Keeney, N. Kim, T. H. Koch, S. Kraemer, L. Kroiss, N. Le, D. Levine, W. Lindsey, B. Lollo, W. Mayfield, M. Mehan, R. Mehler, S. K. Nelson, M. Nelson, D. Nieuwlandt, M. Nikrad, U. Ochsner, R. M. Ostroff, M. Otis, T. Parker, S. Pietrasiewicz, D. I. Resnicow, J. Rohloff, G. Sanders, S. Sattin, D. Schneider, B. Singer, M. Stanton, A. Sterkel, A. Stewart, S. Stratford, J. D. Vaught, M. Vrkljan, J. J. Walker, M. Watrobka, S. Waugh, A. Weiss, S. K. Wilcox, A. Wolfson, S. K. Wolk, C. Zhang and D. Zichi, *PLoS One*, 2010, **5**, e15004.
11 S. Kraemer, J. D. Vaught, C. Bock, L. Gold, E. Katilius, T. R. Keeney, N. Kim, N. A. Saccomano, S. K. Wilcox, D. Zichi and G. M. Sanders, *PLoS One*, 2011, **6**, e26332.
12 F. Teles and L. Fonseca, *Talanta*, 2008, **77**, 606–623.
13 P. Hegde, R. Qi, K. Abernathy, C. Gay, S. Dharap, R. Gaspard, J. E. Hughes, E. Snesrud, N. Lee and J. Quackenbush, *BioTechniques*, 2000, **29**, 548–562.
14 V. G. Cheung, M. Morley, F. Aguilar, A. Massimi, R. Kucherlapati and G. Childs, *Nat. Genet.*, 1999, **21**, 15–19.
15 C. Situma, M. Hashimoto and S. A. Soper, *Biomol. Eng.*, 2006, **23**, 213–231.
16 K. Pappaert, P. Van Hummelen, J. Vanderhoeven, G. V. Baron and G. Desmet, *Chem. Eng. Sci.*, 2003, **58**, 4921–4930.
17 L. Wang and P. C. Li, *Anal. Chim. Acta*, 2011, **687**, 12–27.
18 M. K. McQuain, K. Seale, J. Peek, T. S. Fisher, S. Levy, M. A. Stremler and F. R. Haselton, *Anal. Biochem.*, 2004, **325**, 215–226.
19 J. Liu, B. A. Williams, R. M. Gwirtz, B. J. Wold and S. Quake, *Angew. Chem., Int. Ed.*, 2006, **45**, 3618–3623.
20 P. K. Yuen, G. Li, Y. Bao and U. R. Muller, *Lab Chip*, 2003, **3**, 46–50.
21 C.-W. Wei, J.-Y. Cheng, C.-T. Huang, M.-H. Yen and T.-H. Young, *Nucleic Acids Res.*, 2005, **33**, e78.
22 R. H. Liu, R. Lenigk, R. L. Druyor-Sanchez, J. Yang and P. Grodzinski, *Anal. Chem.*, 2003, **75**, 1911–1917.
23 J. Rupp, M. Schmidt, S. Münch, M. Cavalar, U. Steller, J. Steigert, M. Stumber, C. Dorrer, P. Rothacher, R. Zengerle and M. Daub, *Lab Chip*, 2012, **12**, 1384–1388.
24 L. Wang and P. C. H. Li, *Anal. Biochem.*, 2010, **400**, 282–288.
25 R. Peytavi, F. R. Raymond, D. Gagné, F. J. Picard, G. Jia, J. Zoval, M. Madou, K. Boissinot, M. Boissinot, L. Bissonnette, M. Ouellette and M. G. Bergeron, *Clin. Chem.*, 2005, **51**, 1836–1844.
26 H. Chen, L. Wang and P. C. H. Li, *Lab Chip*, 2008, **8**, 826–829.

27 X. Wang, X. Chen, X. Ma, X. Kong, Z. Xu and J. Wang, *Talanta*, 2011, **84**, 565–571.
28 N. B. Adey, M. Lei, M. T. Howard, J. D. Jensen, D. A. Mayo, D. L. Butel, S. C. Coffin, T. C. Moyer, D. E. Slade, M. K. Spute, A. M. Hancock, G. T. Eisenhoffer, B. K. Dalley and M. R. McNeely, *Anal. Chem.*, 2002, **74**, 6413–6417.
29 D. Erickson, X. Liu, U. Krull and D. Li, *Anal. Chem.*, 2004, **76**, 7269–7277.
30 Y. Gao, L. K. Wolf and R. M. Georgiadis, *Nucleic Acids Res.*, 2006, **34**, 3370–3377.
31 Y. Okahata, M. Kawase, K. Niikura, F. Ohtake, H. Furusawa and Y. Ebara, *Anal. Chem.*, 1998, **70**, 1288–1296.
32 C. F. Edman, D. E. Raymond, D. J. Wu, E. Tu, R. G. Sosnowski, W. F. Butler, M. Nerenberg and M. J. Heller, *Nucleic Acids Res.*, 1997, **25**, 4907–4914.
33 G. Garcia-Schwarz, M. Bercovici, L. A. Marshall and J. G. Santiago, *J. Fluid Mech.*, 2011, **679**, 455–475.
34 A. Persat and J. G. Santiago, *Anal. Chem.*, 2011, **83**, 2310–2316.
35 M. Bercovici, G. V. Kaigala, K. E. Mach, C. M. Han, J. C. Liao and J. G. Santiago, *Anal. Chem.*, 2011, **83**, 4110–4117.
36 M. Bercovici, C. M. Han, J. C. Liao and J. G. Santiago, *Proc. Natl. Acad. Sci. U. S. A.*, 2012, **109**, 11127–11132.
37 S. S. Bahga, C. M. Han and J. G. Santiago, *Analyst*, 2013, **138**, 87–90.
38 G. Garcia-Schwarz and J. G. Santiago, *Anal. Chem.*, 2012, **84**, 6366–6369.
39 G. Garcia-Schwarz and J. G. Santiago, *Angew. Chem., Int. Ed.*, 2013, **52**, 11534–11537.
40 M. Karsenty, S. Rubin and M. Bercovici, *Anal. Chem.*, 2014, **86**, 3028–3036.
41 V. Shkolnikov and J. G. Santiago, *Anal. Chem.*, in press.
42 T. K. Khurana and J. G. Santiago, *Anal. Chem.*, 2008, **80**, 6300–6307.
43 A. Rogacs, L. A. Marshall and J. G. Santiago, *J. Chromatogr. A*, 2014, **1335C**, 105–120.
44 A. Persat and J. G. Santiago, *New J. Phys.*, 2009, **11**, 075026.
45 R. Levicky and A. Horgan, *Trends Biotechnol.*, 2005, **23**, 143–149.
46 R. A. Vijayendran, F. S. Ligler and D. E. Leckband, *Anal. Chem.*, 1999, **71**, 5405–5412.
47 T. M. Phillips, J. A. Thompson and H. H. Bau, *J. Chromatogr. B: Anal. Technol. Biomed. Life Sci.*, 2010, **878**, 228–236.
48 M. F. Hagan and A. K. Chakraborty, *J. Chem. Phys.*, 2004, **120**, 4958–4968.
49 G. Bhanot, Y. Louzoun, J. Zhu and C. DeLisi, *Biophys. J.*, 2003, **84**, 124–135.
50 M. Sartor, J. Schwanekamp, D. Halbleib, I. Mohamed, S. Karyala, M. Medvedovic and C. R. Tomlinson, *BioTechniques*, 2004, **36**, 790–796.
51 K. Pappaert and G. Desmet, *J. Biotechnol.*, 2006, **123**, 381–396.
52 V. Chan, D. J. Graves and S. E. McKenzie, *Biophys. J.*, 1995, **69**, 2243–2255.
53 A. E. Nkodo, J. M. Garnier, B. Tinland, H. Ren, C. Desruisseaux, L. C. McCormick, G. Drouin and G. W. Slater, *Electrophoresis*, 2001, **22**, 2424–2432.
54 M. Vadnere, G. Amidon, S. Lindenbaum and J. L. Haslam, *Int. J. Pharm.*, 1984, **22**, 207–218.
55 L. A. Marshall, A. Rogacs, C. Meinhart and J. G. Santiago, *Proceedings of American Institute of Chemical Engineers Annual Meeting*, San Francisco, 2013.
56 J. I. Molho, A. E. Herr, B. P. Mosier, J. G. Santiago, T. W. Kenny, R. A. Brennen, G. B. Gordon and B. Mohammadi, *Anal. Chem.*, 2001, **73**, 1350–1360.
57 A. Spehar, S. Koster, V. Linder, S. Kulmala, N. F. de Rooij, E. Verpoorte, H. Sigrist and W. Thormann, *Electrophoresis*, 2003, **24**, 3674–3678.
58 M. R. Henry, P. Wilkins Stevens, J. Sun and D. M. Kelso, *Anal. Biochem.*, 1999, **276**, 204–214.
59 K. Tawa and W. Knoll, *Nucleic Acids Res.*, 2004, **32**, 2372–2377.
60 C. Gadgil, A. Yeckel, J. J. Derby and W.-S. Hu, *J. Biotechnol.*, 2004, **114**, 31–45.

